MINERALOGICAL MAGAZINE

VOLUME 38 NUMBER 295 SEPTEMBER 1971

Yttrotungstite

R. J. DAVIS

Mineralogy Department, British Museum (Natural History), Cromwell Road, London, S.W. 7

AND G. W. SMITH

British Petroleum Co. Ltd., B.P. Research Centre, Sunbury-on-Thames, Middlesex

SUMMARY. Yttrotungstite occurs at Kramat Pulai mine, and at Tapah, Kinta, Perak, Malaysia, as yellow earthy material and as monoclinic laths, elongated along [001], flattened, and always twinned, on {100} to pseudo-orthorhombic symmetry, and frequently bevelled by {110}; crystals are very rarely terminated by {101}. γ = [010], α:[001] = 26°, probably in β acute, and $2V_\alpha \simeq 68°$. A thermal weight loss curve and an infra-red absorption spectrum are given and discussed. Accessory minerals include raspite and stolzite.

The yttrotungstite unit cell has a 6·95, b 8·64, c 5·77, β 104° 56′, space group $P2_1/m$; cell contents are $(Yt, Ln, Ca, Mg)_2(W, Al, Si, Ti, Fe)_4(O, OH)_{14}(OH)_2.2H_2O$. Indexed X-ray powder data are given. Microprobe studies show that Al and Si replace W and are concentrated in zones showing larger values of $a \sin\beta$ (6·75 Å instead of 6·72 Å) but with no other appreciable difference in cell dimensions. Crystal structure studies show that the structure consists of WO_6 octahedra sharing non-opposite edges in zig-zag chains running parallel to [010]. Yttrium is in approximately trigonal prismatic coordination between the chains, with the water molecule as a seventh neighbour at one prism face. The water molecule is accommodated in the angle between zig-zags in the WO_6 chains; it is probably hydrogen bonded to chain oxygen atoms, and becomes coordinated to the yttrium by a shear between chains away from strict close-packing of the oxygen atoms. The shear is related to the change in $a \sin\beta$ in (Al, Si)-rich zones; arguments based on this and on details of the chemical analysis suggest that SiO_4 replaces WO_6 with a local oxygen deficit.

Oxygen atom peaks on partial Fourier difference syntheses for our data for yttrotungstite are only slightly larger than the troughs in the syntheses due to experimental error. Methods of testing the significance of the positive peaks are described in an appendix.

SCRIVENOR and Shenton (1927) described thorotungstite, occurring as shapeless blocks at the base of a tin-bearing alluvial deposit overlying tourmaline granite at the Kramat Pulai mine, Pulai, Kinta district, Perak, Malaysia. The name was given on the basis of a chemical analysis showing ThO_2 and WO_3 as the main constituents; Beard (1950)[1] referred to a new unpublished analysis of material from the type locality showing that what was taken to be ThO_2 by Shenton in fact consists of rare earths, dominantly yttria. Beard proposed the revised name *yttrotungstite* for this mineral, a name that is now accepted.

[1] Butler (1957) gives the author of this reference as E. H. Bradshaw, while Semenov *et al.* (1965) attribute it to R. Bradshaw. In fact it was published over the initials E. H. B. and was written by Dr. E. H. Beard, the editor of the journal. The analysis has subsequently been published by Bradford (1961).

Butler (1957) analysed the rare earths in a specimen of yttrotungstite from the type locality, from Dr. Bradshaw of the Malay Geological Survey. He found that while yttria dominated the analysis and lanthanons of even atomic number predominated over those of odd atomic number, the concentration variations within each class were relatively small. Semenov, Kataeva, and Rudnitskaya (1965) examined Butler's sample[1] and gave a full chemical analysis, additional rare earth analyses, X-ray powder data, optical properties, D.T.A. and weight-loss heating curves, and an infra-red absorption spectrum. They suggested the formulae[2] $Yt_2W_5O_{14}(OH)_8$ or $YtW_3O_9(OH)_3$.

The authors independently undertook X-ray studies of yttrotungstite. Our results when compared were in satisfactory agreement and we were able jointly to derive the crystal structure of yttrotungstite and a more satisfactory formula. We are grateful to many colleagues for further details of its physical properties.

Specimens. We have studied all specimens of yttrotungstite in the British Museum (Natural History) collection, namely B.M.1921,395, B.M.1927,1157–60, B.M.1948, 435, and B.M.1969,165–70, all from the type locality. We have also studied GR.740, collected by Dr. G. V. Wood from a mine dump at Tapah, Kinta district, Perak, Malaysia. A portion of this sample has been presented to the British Museum (Natural History) collection as B.M.1969,227.

All the specimens studied consisted mainly of a fine-grained aggregate of pale-yellow earthy yttrotungstite, with rare druses lined by yttrotungstite crystals. The yttrotungstite was sometimes admixed with large rounded quartz grains. Both earthy and crystalline yttrotungstite gave the same characteristic X-ray powder pattern as was given[3] by the samples of analysed material referred to by Beard (1950).

In a survey of accessory minerals, J. G. Francis and Miss E. E. Fejer have identified by X-ray powder photographs: frequent patches of white earthy kaolinite, also quartz, muscovite, hydrobiotite, illite, haematite, and a new mineral, which has proved to be the aluminium analogue of ferritungstite. Rare, probably allogenic, crystals of tourmaline, scheelite, rutile, and cassiterite were identified; cassiterite also occurred as yellow earthy varlamoffite. Fine grained stolzite and raspite were identified, raspite being also present as crystals in the druses. The associated minerals agree well with the description given by Bradford (1961) of the paragenesis of tin and tungsten ores especially at Kramat Pulai.

Crystals from GR.740 and B.M.1927,1157 were selected for detailed study. Several grams of earthy yttrotungstite from B.M.1927,1157 were crushed through 300 mesh; this material will be referred to below as Sample E. X-ray powder photographs (11·46 cm diameter camera) showed that Sample E was essentially pure yttrotungstite, but on diffractometer traces and focusing-camera photographs it was possible to observe a few extremely weak extra lines. Some of these could be attributed to a few per cent of the aluminium analogue of ferritungstite, and a weak sharp line at 7·2 Å

[1] Semenov *et al.* (1965) state that their sample was No. 3306 from the British Museum. No specimen of yttrotungstite answers this description in the British Museum (Natural History) collection and Dr. Butler confirms that their specimen was a portion of the material he studied.

[2] At the editor's suggestion we use here the old symbol, Yt, for yttrium to avoid confusion with Y used as an algebraic symbol or to indicate an atomic site.

[3] Films X4658, X4660, ref. M 5419/37, British Museum (Natural History).

was attributed to a trace of kaolinite. Mr. R. F. Symes has isolated a minute fraction of sample E that floated at 3·2 gm/cm³. This consists dominantly of white grains of a fine-grained intergrowth (smooth powder lines) of yttrotungstite with muscovite or more probably illite. Traces of quartz, calcic plagioclase, and gypsum were also identified in the floating fraction.

X-ray data. Oscillation, rotation, and equi-inclination Weissenberg photographs show that the crystals of yttrotungstite are monoclinic, space group $P2_1$ or $P2_1/m$. We derive below a satisfactory structure for yttrotungstite in $P2_1/m$. All the crystals were laths, flattened on {100} and elongated along [001], and poorly oriented, showing a mosaic spread of at least 4°. All the crystals studied (about 40) were twinned on {100}; this accounts for the orthorhombic symmetry reported by Scrivenor and Shenton. Characteristic effects on all Weissenberg photographs around [001] and [010] except

TABLE I. *Yttrotungstite cell dimension measurements. Figures given in brackets are estimated errors in the last unbracketed digit (in col. 1 the error is the 95 % confidence limit = 2·15σ)*

	1	2	3	4	5	6
a	6·954(6) Å	—	—	—	—	—
b	8·637(9) Å	8·632(2)	8·633(3)	8·631(2)	8·635(3)	8·627(2)
c	5·771(6) Å	—	—	—	—	—
β	104° 56′(4)	—	105° 7′(4)	105° 4′(5)	105° 4′(7)	105° 0′(4)
a sin β	6·718(7) Å	6·714(3)	6·718(3)	{6·715(3) {6·750(6)	6·718(2) 6·748(5)	6·715(4) 6·746(8)
c sin β	5·576(6) Å	—	5·572(4)	5·575(2)	5·580(4)	5·578(4)
V	334·8(7) Å³	—	—	—	—	—

1. Mean of two determinations on Sample E, agreeing to 0·02 %, in a Nonius de Wolff focusing camera using Cu-$K\alpha$ radiation and the lines detailed in table II. Calibrated samples of SnO_2 and NH_4Cl respectively were used as internal standards. Measurements were refined by Hess's (1951) least-squares method, assuming unknown film shrinkage errors and camera errors in 2θ proportional to tan 2θ.

2 to 6. Results by Farquhar and Lipson's (1946) method from pairs of symmetrical back reflection oscillation photographs taken around *c* and *b* for crystals from B.M.1927,1157. β was derived from the *b*-axis oscillation photograph taken along *c*, and is thus an average value for the two lattices in the peristerite effect, whose separate reflections were not resolved on this photograph.

for (*hk*o) showed that the twinning was on a gross scale, with opposite faces of the laths belonging predominantly to opposite twins.

Cell dimension data for yttrotungstite are given in table I. Data from Sample E (col. 1) and for the first two crystals (cols. 2 and 3) are in excellent agreement. However, many yttrotungstite crystals showed a peristerite[1] effect in which high-angle reflections near a^* were resolved into two α_1/α_2 doublets indicating two lattices in parallel orientation with the same *b* and *c* dimensions but differing slightly in *a* sin β.

[1] Name given by analogy with the crystallographically similar effect of this name observed in feldspars.

From table I, the lattice common to all crystals has the same dimensions as the earthy material, and the second, larger lattice occurs only in certain crystals.[1]

Powder data, indexed with the help of single crystal intensities, are given in table II and are more complete than those of Semenov *et al.*, who used a smaller camera.

TABLE II. *X-ray powder data for yttrotungstite; yellow-brown laths from B.M.1927, 1157, Kramat Pulai mine, Kinta, Perak, Malaysia; film 748Fa taken in an 11·46 cm diameter camera with filtered* Cu-$K\alpha$ *radiation*

d_{obs}	I	d_{calc}	hkl	d_{obs}	I	d_{calc}	hkl	d_{obs}	I	d_{obs}	I
6·73 Å	ms	6·716 Å	100*	2·554 Å	mw	2·557 Å	031*	1·990 Å	mwB	1·284 Å	m
5·57	mw	5·576	001*	—	—	2·491	$13\bar{1}$†	1·914	w	1·260	mw
—	—	5·301	110†	2·486	m	2·486	$20\bar{2}$‡	1·872	w	1·246	w
4·98	s	4·972	$10\bar{1}$*	—	—	2·484	211†	1·828	mw	1·226	vvw
4·69	vvs(2)	4·684	011*	—	—	2·389	$21\bar{2}$†	1·796	mw	1·205	mw
4·32	mw	4·317	020§	—	—	2·379	$12\bar{2}$†	1·760	mw	1·188	w
—	—	4·309	$11\bar{1}$†	2·375	vvw	2·366	102	1·737	mw	1·169	vw
3·83	m	3·829	101*	—	—	2·342	022†	1·707	w	1·152	vwB
3·63	m	3·631	120*	2·302	w	2·300	131	1·678	vvw	1·136	vw
3·51	vw	3·500	111*			2·294	$30\bar{1}$	1·652	ms	1·110	mw
—	—	3·413	021†	—	—	2·282	112†	1·609	vvw	1·094	w
3·36	ms	3·358	200*	2·239	m	2·239	300*	1·594	m	1·085	mw
3·26	vvs(1)	3·278	$20\bar{1}$	—	—	2·223	221‖	1·571	wB	1·064	vw
		3·260	$12\bar{1}$	—	—	2·217	$31\bar{1}$†	1·534		1·054	w
3·13	w	3·130	210*	—	—	2·185	230†	1·528	mw	1·039	mw
3·07	m	3·064	$21\bar{1}$*	—	—	2·167	310†	1·505	w	1·027	vvw
2·869	ms	2·864	121	—	—	2·163	$23\bar{1}$†	1·473	mwB	1·013	vvw
—	—	2·851	$10\bar{2}$†	2·159	w	2·158	040	1·455	w	0·984	vvw
2·790	ms	2·788	002*	—	—	2·154	$22\bar{2}$†	1·438	mw	0·975	vw
—	—	2·707	$11\bar{2}$†	2·079	w	2·075	122*	1·421	w	0·957	mwB
—	—	2·653	012†	—	—	2·055	140†	1·395	vw	0·938	mwB
2·650	ms	2·650	220			2·026	$32\bar{1}$	1·381	vvw	0·907	mwB
		2·645	130‡	2·028	vs(3)	2·025	$13\bar{2}$	1·350	vvw		
—	—	2·611	$22\bar{1}$†			2·021	$30\bar{2}$	1·322	vwB		
2·597	mw	2·594	201‡	—	—	2·013	041†	1·296	vw		

* Lines used for cell dimension determination (see table I, col. 1) and for intensity measurements (see below).
† Reflections weak or absent on single crystal photographs.
‡ Lines used for cell dimensions only.
§ Line used for intensities only.
‖ The 221 reflection appeared extremely weakly on focusing camera photographs and was used for cell dimension determination.

Diffractometer traces of Sample E showed evidence of preferred orientation in which the c axis, and to a slightly lesser extent the b axis, tended to lie in the plane of the specimen surface, even when the powder was dispersed in plastic, suggesting that the fine-grained material is morphologically similar to the crystals.

[1] The difference in $a \sin \beta$ between the two lattices is such that if the second lattice were present in Sample E it would give rise to easily resolvable doublets on focusing camera photographs.

Microprobe studies were made by Dr. S. J. B. Reed and Mr. R. F. Symes on crystals from B.M.1927,1157, using a Cambridge Geoscan. Twenty-one crystals were sorted, using X-ray back reflection oscillation photographs with the beam nearly perpendicular to (100), into three classes: four *one-lattice* crystals showing no evidence of the second yttrotungstite lattice: ten *intermediate* crystals showing the second lattice weakly: and seven *peristeritic* crystals showing the second lattice as strongly as the first. The crystals were mounted on Durofix and examined in the Geoscan without polishing.

Forty-one measurements of the ratio of X-ray intensities from tungsten and yttrium respectively ($L\alpha_1$ lines at 25 kV, corrected for background) gave means and standard deviations showing no significant difference between the three classes. The peristerite phenomenon is therefore probably unconnected with major constituents such as these elements or the lanthanons.

Twenty-four measurements of the contents of Al and Si, using $K\alpha$ X-ray lines at 20 kV, were expressed uncorrected as wt % oxides relative to a topaz standard; corrected results might be higher by a factor of up to 1·5. About half the results showed $<0{\cdot}05$ wt % Al_2O_3, with SiO_2 in the range 0·3–0·7 wt %; the remainder showed comparable amounts of Al_2O_3 and SiO_2 ranging up to 7·3 wt % Al_2O_3 and 11·1 wt % SiO_2 in peristeritic crystal 3. Scanning photographs of this crystal in fig. 1 show high local concentrations of Al and Si coinciding on the crystal surface. Further scanning photographs of four crystals from each class showed perfect correlation with the peristerite effect: one-lattice crystals showed virtually no Al,Si concentrations; intermediate crystals showed small concentrations; peristeritic crystals showed extensive Al,Si concentrations. Al and Si concentrations always coincided. Ca and Mg showed no concentrations within the crystals. A typical line scan across an Al,Si concentration is shown in fig. 2a, taken from the crystal of fig. 1. The traces for Al and Si rise simultaneously to about the same extent, indicating *ca.* 10 wt % of each oxide, and wherever this happens the traces for both W and Yt fall.

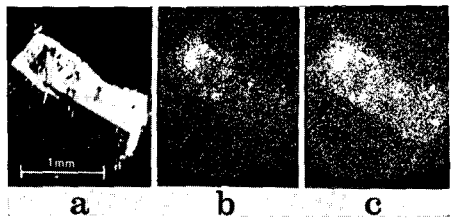

FIG. 1. Scanning photographs of peristerite-type crystal 3 from B.M.1927,1157. (a) Secondary electrons from the crystal. The scale mark should read 0·1 mm. (b) Al-$K\alpha$ radiation. (c) Si-$K\alpha$ radiation.

The peristerite phenomenon is thus associated with high surface concentrations of Al and Si, but the amounts found are far too large to be accommodated in the yttrotungstite lattice and thus apparently indicate a second phase. Moreover, despite the Yt trace in fig. 2a, it is crystallochemically impossible for Al and Si to replace an atom as large as Yt. However, with concentrations as large as those shown in fig. 1, if the second phase extends to any depth it should give evidence on the X-ray single crystal photographs; such evidence was not observed. These high concentrations of Al and Si thus represent a thin surface layer only. A rough calculation shows that an aluminosilicate layer about 0·1 μm thick would give apparent oxide concentrations of several per cent, and would reduce the intensity of the Yt-$L\alpha_1$ line from the underlying yttrium by about 10 %, relative to the W-$L\alpha_1$ line intensity. This model thus

explains the constancy of the W:Yt ratio found above, without postulating the replacement of Yt by Al and Si.

Five yttrotungstite crystals (not examined by X-rays) were polished to show their internal cross-section. Scanning photographs showed coincident Al,Si concentrations on some of the crystals, entirely confined to the crystal edges. Twenty-four measurements on two crystals away from the Al,Si concentrations, showed a uniform content

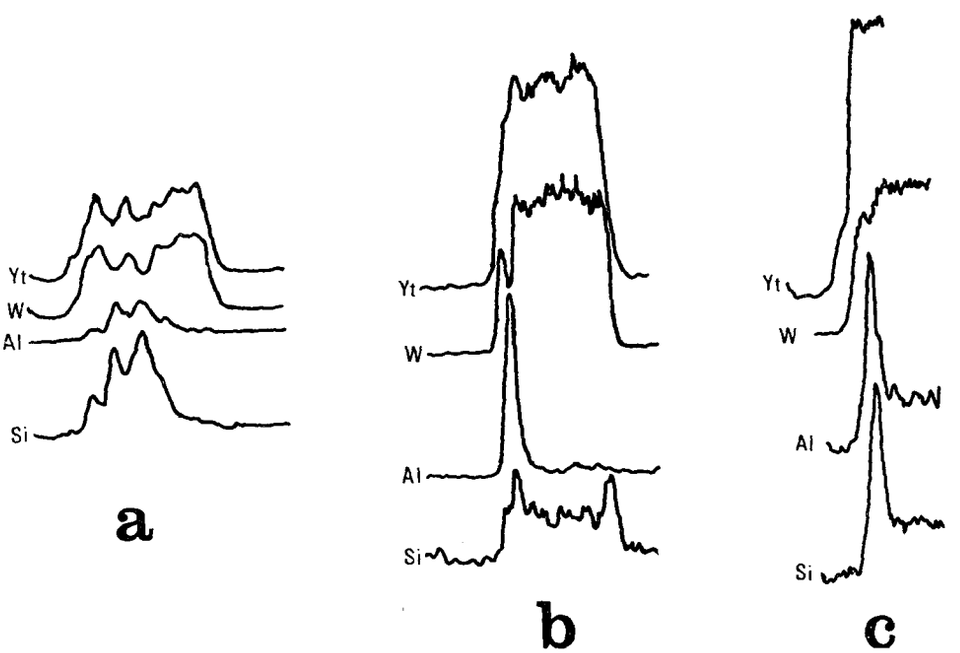

FIG. 2. Line scans across three crystals of yttrotungstite from B.M.1927,1157, made with Yt-$L\alpha_1$, W-$L\alpha_1$, Al-$K\alpha$, and Si-$K\alpha$ radiations respectively. The horizontal scales in each of (a) to (c) are arbitrary and different arbitrary vertical scales are used for each of the twelve traces. (a) scan across surface of crystal 3 illustrated in fig. 1. (b) scan across edge of a polished section through crystal 4/3. (c) similar scan across the edge of crystal 4/2.

of 0·2 wt % SiO_2 (uncorrected), qualitatively confirming the surface measurements. A number of line scans across Al,Si concentrations showed the same features, but none was ideal owing to the proximity to the edge of the crystal and possible edge effects. The scan of fig. 2b shows clearly that where the Al trace rises sharply the W trace dips while the Yt trace is unaffected. The Si trace rises unusually little on this scan, and is more typical in fig. 2c, which shows the same effects otherwise as fig. 2b, but less convincingly distinguished from edge-effects.

Figs. 2b and 2c show that beneath the thin aluminosilicate surface layer postulated above are yttrotungstite zones enriched in Al and Si replacing W. These zones explain the presence of the second yttrotungstite lattice and occur only in the surface layers of the crystals; since the crystals are highly absorbing to X-rays, only their surface

layers diffract, and X-ray single crystal photographs exaggerate the overall content of (Al,Si)-rich zones. The sharpness of the X-ray reflections from the second yttrotungstite lattice shows that the zones are of very uniform composition, suggesting that this is defined by solid solubility limits, probably of Si in yttrotungstite.

This work provides proof, for the first time, that Si (as well as Al) can replace W in tungstate minerals.

From the results obtained above from X-ray focusing camera photographs of Sample E, the (Al,Si)-rich zones are absent from the earthy material and must have become incorporated into the large yttrotungstite crystals as they recrystallized around the druses in the earthy matrix. The temperature of this process is limited by the observation of crystals of raspite in the druses; raspite inverts rapidly to stolzite[1] at 410 °C.

The Al and Si are probably derived from clay minerals. These may have been imported with the ground water from the alluvial layer overlying the yttrotungstite *in situ*. Alternatively the clay is the illite (or muscovite) observed in Sample E. The thin surface film of aluminosilicate may be a residue of unabsorbed clay or alternatively be attributed to etching by relatively acid ground-water. Any complete explanation of the (Al,Si)-rich zones must also explain why they are confined to the surface layers of the yttrotungstite crystals.

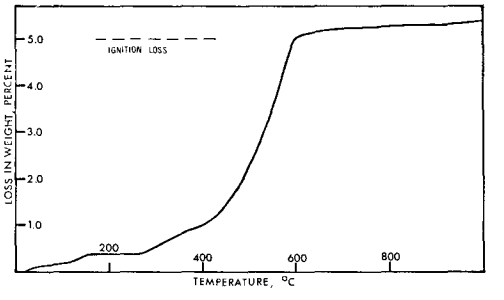

FIG. 3. Weight-loss curve obtained on 163 mg of sample E in a Stanton Thermobalance. The ignition loss, obtained by Dr. A. A. Moss in a partial analysis of this sample, is shown for comparison

Heating experiments. Fig. 3 shows a weight-loss heating curve obtained by Mr. C. J. Elliott, which agrees well with that of Semenov *et al.* The weight-loss occurs in two stages: about 0·4 % is lost at temperatures up to 150 °C, and the remaining 4·8 % is lost between 250° and 600 °C, mainly above 400 °C. This behaviour is very similar to that of the clay impurities found in Sample E, which lose adsorbed water at 150 °C but retain structural water up to 500 °C.

The infra-red spectrum of fig. 4 was obtained by Mr. C. J. Elliott. A similar spectrum was obtained from crystals of GR.740. The spectra are in good agreement with that given by Semenov *et al.* but are extended to lower and higher wavelengths. Semenov *et al.* attribute the strong absorptions in the range 9 to 14 μm to W–O vibrations, since they are similar to those found in the spectra of tungsten hetero-poly acids. However, their assignment of the small peak at 1440 cm^{-1} (6·94 μm) to OH stretching vibrations appears to be a mistake, since these usually absorb in the range 2·85–2·90 μm (here 2·87 μm) while the peak at 6·1 μm in fig. 4 is attributable to H–O–H bending vibrations. This last peak shows that at least some of the hydrogen in yttrotungstite is in the form of discrete water molecules. The identity of these peaks was verified

[1] G. F. Claringbull and D. McKie, unpublished work, X 6363.

on a portion of sample E heated 7 hours at 130 °C, when the spectrum was unchanged, and on the sample used for the thermobalance experiment to 750 °C when these peaks were eliminated and the spectrum completely changed. Mr. Elliott also noted the small peak at 3·35 μm, which resembles that attributed to 'co-ordinated water' in the infra-red spectrum of $LiOH.H_2O$ by Jones (1954), and the presence of this peak was verified at a higher sample concentration.

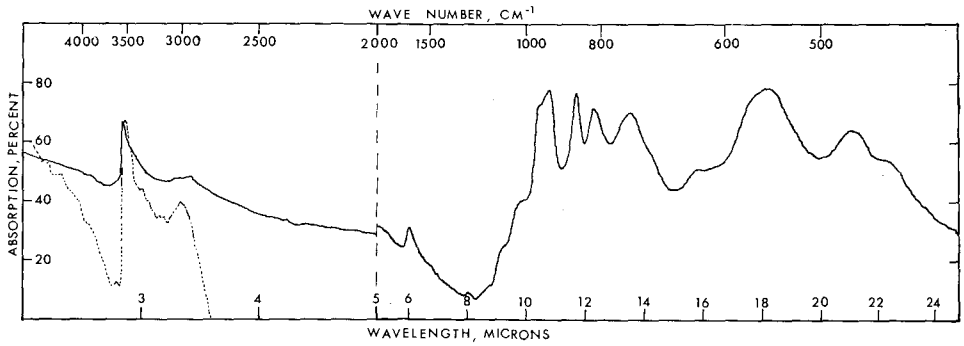

FIG. 4. Infra-red absorption spectrum No. 1332 obtained for Sample E using a Grubb Parsons Spectromaster. For the solid curve the sample was at 0·5 wt % concentration in a KBr disc; for the dotted curve the sample was at 3 wt % concentration.

Morphology. Crystals from our specimens were too small to measure goniometrically. Like the crystals figured by Scrivenor and Shenton (their fig. 1), many of our lath-like crystals were sharply bevelled on their long edges. Seven measurements in silhouette on two mounted crystals gave the angle 36·9 $\pm 3°$, which identifies the bevelling face as (110) [(110):(100) = 37·9°]. Terminal faces as shown in Scrivenor and Shenton's fig. 1 were extremely rare on our material and we have found only one crystal from B.M.1921,395 showing such a face. Two independent settings gave angles of 57° and 60° in silhouette. An X-ray oscillation photograph was too poor to identify whether the face-normal lay in β acute or β obtuse, but the only simple face fitting these measurements is $(10\bar{1})$ [$(10\bar{1})$:(100) = 59·4°].

Cleavage. We have verified the presence of the two cleavages given by Scrivenor and Shenton. That running along the laths is (010); that running across the laths is less well defined, due to the twinning, but structural results below suggest that it probably lies on $(10\bar{1})$.

Specific gravity. Dr. R. Walls found D 5·96 on crystals from GR.740 (Berman balance) and we accept this as the most reliable value. Earlier results (5·85, Semenov *et al.*; 5·55, Scrivenor and Shenton) are presumably on impure earthy material. Mr. A. J. Easton found D 5·55 pyknometrically on Sample E; if this contained, say, 5·8 % kaolinite, the corrected specific gravity would become 5·96.

Optical properties. Semenov *et al.* obtained α 1·89 pale yellow, β 1·98, γ 2·02 dark yellow, on earthy material. Mr. P. G. Embrey found that crystals from GR.740 were length fast, had a birefringence about 0·12 and probably gave a β-axis interference

figure, whence γ = [010] and α is near [001]. On a very thin section of GR.740 Dr. A. C. Bishop observed repeated gross twinning with α:[001] 26°, and estimated $2V_\alpha$ 68° (cf. $2V_\alpha$ (calc.) 65° from data above).

Chemical analyses. Scrivenor and Shenton's (1927) analysis of 'thorotungstite' was defective and they do not state specifically that it was obtained from crystals. The only reliable analysis is that given by L. C. Chadwick for hand-picked crystals (table III,

TABLE III. *Unit cell contents of yttrotungstite*

	1	3		1	2	3		1	2	3
WO_3	71·45 %	3·70	Ce_2O_3	2·21	2·06	0·15	Gd_2O_3		1·27	0·08
Fe_2O_3	0·36	0·06	La_2O_3		0·28	0·02	Tb_2O_3		0·23	0·02
Al_2O_3	0·87	0·21	Pr_2O_3		0·33	0·02	Dy_2O_3		1·38	0·09
TiO_2	0·01	0·00	Nd_2O_3	3·80	2·33	0·17	Er_2O_3	15·52	1·15	0·07
SiO_2	0·37	0·07	Sm_2O_3		0·76	0·05	Tm_2O_3		0·14	0·01
MgO	0·17	0·05	Eu_2O_3		—	—	Yb_2O_3		1·18	0·07
CaO	0·32	0·07	Sum		3·70		Lu_2O_3		0·13	0·01
			La to Eu				Yt_2O_3		10·29	1·10
							Sum		15·77	
Atom totals							Gd to Yt			
W to Si		4·04					H_2O^+	4·96		6·62
Mg to Yt		1·98					H_2O^-	0·07		—
H		6·62					Sum	100·11	21·53	
O		17·86								

Col. 1. L. C. Chadwick's analysis on hand-picked crystals (Bradford, 1961).
Col. 2. Ratios of rare earths, converted to sesquioxides, after Butler (1957), but normalized to the total rare earths (21·53 %) found in col. 1.
Col. 3. Atoms per unit cell of volume 334·9 Å^3, for a density of 5·96 gm/cm^3.

col. 1). Semenov *et al.* (1965) analysed earthy material having significantly higher contents of Al_2O_3 and SiO_2, which could be explained by the presence of about 3 % kaolinite (cf. 5·8 % kaolinite from the density of Sample E above). An unpublished analysis for earthy material by Chadwick (E. H. Beard, pers. comm.) gives Al_2O_3 1·19 %, SiO_2 1·14 % (cf. table III).

Chadwick gives only grouped rare earth contents, probably based on the relative solubilities of the double sulphates with potassium. Table III, col. 2 gives the analysis of Butler (1957) on 18·96 % rare earths from earthy yttrotungstite, renormalized to the total found by Chadwick on the purer material. The grouped totals for the Butler data are in excellent agreement with those found by Chadwick.

Chadwick attributes his silica to traces of quartz in the sample analysed. Our microprobe studies show that there is silicon in the yttrotungstite crystals and we have accordingly included silica in the analysis in table III. The microprobe also shows that aluminium is confined to local concentrations in the crystals, thought to correspond to the peristerite effect. Both the crystals used for X-ray structural studies below showed the peristerite effect, and we have therefore included the aluminium in the analysis to give the average composition of the crystals.

We calculate atoms per unit cell in table III, col. 3. Oxygen atoms total 18 almost

exactly (but see below), and, guided by the structural results and cation radii from the literature, there are four atoms per cell consisting mainly of tungsten and two consisting of yttrium and rare earths. From the cation radii, silicon can only replace tungsten, as found by microprobe, like the aluminium, iron, and titanium; calcium belongs with the rare earths and magnesium is a borderline case, which we have arbitrarily allotted to the rare earths. We conclude that the true formula of yttrotungstite is $(Yt,Ln,Ca,etc.)_2(W,Fe,Si,Al,Ti)_4(O,OH,H_2O)_{18}$, where, from infra-red studies, at least some of the hydrogen must be attributed to water molecules.

Crystal structure

Experimental. From crystals from B.M.1927,1157 and GR.740 we have collected visual estimates of reflection intensities for *hk*o (two sets), *h*o*l*, and o*kl* reflections, as listed in table IV. *hk*o data were unaffected by twinning; for *h*o*l* data contributions from the two halves of the twin were summed; o*kl* data were uncorrected for twinning. Only Lorentz-polarization corrections were applied; other errors, such as α_1/α_2 resolution, can be neglected since they affect only the apparent temperature factor, *B*. However, the crystals were very non-equiaxed, causing anisotropic absorption of X-rays, which affects the measurements appreciably, as well as the value of *B*.

The original object of this work was to obtain data on the number of heavy-metal-atom positions, as a guide in interpreting table III, and apart from the integrated *hk*o data, no attempt was made to make high-quality measurements. To eliminate anisotropic absorption, data were also collected from X-ray powder photographs (15 unambiguously indexable lines given in table II); our experiments with diffractometer traces from Sample E showed that preferred orientation effects made these useless for collecting intensity data.

Refinements were carried out for each set of data independently, using computer programs written by R. J. D. These programs used four-point interpolation in lists of atomic scattering factors for neutral atoms (anomalous dispersion was neglected); they performed full matrix least-squares refinement of scale and temperature factors, atomic coordinates, and, where desired, fractional occupancies, *n*, of atomic sites.[1] Unobserved reflections were treated as recommended by Dunning and Vand (1969) with $c = 1$. Refinement was continued automatically until the calculated shift in each parameter refined was less than one-tenth of its standard deviation.

The quantity minimized in the refinements was $\Sigma(\Delta F/F_0)^2 = \Sigma(F_{obs}-F_{calc})^2/F_{obs}^2$, which assumes a constant *fractional* error in F_{obs}. Scatter diagrams of refined values of $(\Delta F/F_0)$ against F_{obs}, against $\sin^2\theta$, and on a Weissenberg net showed that the data of table IV, cols. 1 and 3, obeyed this weighting scheme satisfactorily and that much of the residual error was due to anisotropic absorption. Full data in table IV, cols. 2 and 4, showed relatively much larger fractional errors for the weakest reflections with small F_{obs} and comparison of the two equivalent sets of *hk*o data in table IV, cols. 1 and 2, showed that the onset of this larger error was quite sudden at a critical value of F_{obs}. Data in table IV, cols. 2 and 4, were therefore edited to fit the programs

[1] At least one of the site occupancies must be held fixed at a nominal value (usually unity) in order to refine the overall scale factor.

by deleting all reflections, including unobserved ones, whose F_{obs} was less than the critical value.

Heavy atom positions. Unedited data from table IV, cols. 2 and 4, yielded $N(z)$ curves agreeing perfectly with that obtained with a centre of symmetry, suggesting space group $P2_1/m$ rather than $P2_1$; this was verified by Patterson projections of *hk*o and o*kl* data, which showed vectors due to pairs of atoms related by *m*. The Patterson projections of all the single crystal data could be satisfactorily interpreted in terms of a very heavy atom (tungsten) in a four-fold general position, and a moderately heavy

TABLE IV. *Yttrotungstite intensity data and heavy atom positions. Figures given in brackets are standard deviations in the last unbracketed digit*

	1	2	3	4	5	6
	*hk*o	*hk*o	*hol*	o*kl*	Powder	Powder
Film	X 11307	—	X 11358	—	986F	991F
Integrated	Yes	No	No	No	—	—
Observer	A	B	A	B	A	A
No. of reflections:						
Observed	59	49	40	39	15	15
Unobserved	18	—	3	—	—	—
Edited	No	Yes	No	Yes	—	—
n^1_{Yt}	1·46(10)	1·39(13)	1·53(21)	1·30(12)	1·12(11)	1·13(13)
n^2_{Yt}	1·09(8)	1·05(10)	0·98(10)	0·98(7)	0·86(9)	0·87(10)
x_{Yt}	0·720(3)	0·719(4)	0·718(7)	—	0·728(10)	0·725(12)
y_{Yt}	¼	¼	—	¼	¼	¼
z_{Yt}	—	—	0·253(8)	0·257(5)	0·268(17)	0·273(19)
x_W	0·187(1)	0·186(2)	0·182(3)	—	0·178(5)	0·179(6)
y_W	0·062(1)	0·063(2)	—	0·063(2)	0·066(4)	0·067(5)
z_W	—	—	0·203(4)	0·209(2)	0·199(6)	0·196(7)
B Å^2	−0·5(3)	1·9(4)	2·9(14)	1·7(4)	0·2(10)	0·4(11)
R^1	0·191	0·267	0·302	0·171	0·070	0·085
R^2	0·186	0·266	0·303	0·250	0·069	0·085
R^3	0·188	0·317	0·366	0·247	0·064	0·083

Superscripts 1, 2, and 3 refer respectively to refinements carried out: with atomic scattering factors for pure Yt and W; with factors calculated from the cell contents in table IV; with the latter factors but with n_{Yt} (and n_W) held at unity. The same atomic coordinates were obtained in all three refinements, which were all carried out using a single isotropic temperature factor, *B*. *R* values are given for observed reflections only. *hol* data were collected only out to $\theta = 45°$.

atom (yttrium) in a two-fold position on the mirror planes. Partial difference syntheses showed clearly that the tungsten peak was smaller or the yttrium peak was larger (or both) than would be indicated by the atomic scattering factors for pure W and Yt. Believing that only these peaks were identifiable on the syntheses we tried refinements to illustrate this effect, assuming first pure W and Yt, and then the cell contents deduced in table III. The results of the refinements are given in table IV. This table also shows results obtained from measured powder intensities on two films, for which a satisfactory absorption correction could easily be made.

The atomic coordinates obtained in these refinements are all in excellent agreement

(one standard deviation), including the powder data, which shows that the coordinates are unaffected by absorption errors. Values of n^1_{Yt} are all consistently above unity. Since, unlike the atomic coordinates, the site occupancies, n, are linearly related to the structure factors, one can here use Student's t-test to test for significance, and since the refinements were continued to calculated shifts of $0{\cdot}1\sigma$, t is accurate to about 0·1. On this basis, only the values of n^1_{Yt} for the two sets of $hk0$ data differ significantly from unity at the 99 % confidence level. Nevertheless, the values of n^2_{Yt} are all very near unity, and the figures generally support the system of substitutions deduced in table III; atomic scattering factors derived from table III were used in all further refinements.

This method of testing for substitutions is evidently unreliable when, as here, the light atoms are neglected, especially when one of the light atoms overlaps a heavy one in projection. We are surprised how 'robust' these calculations have proved to be, since the values of n^2_{Yt} are very little altered, by only about one standard deviation, when the light atoms are inserted into the refinements (see table V below). Evidently it is not possible to collect sufficient powder intensities to give a significant result, although this would guard against the effect of overlapping light atoms in projections. This effect is in fact quite small, since the atomic scattering factors for heavy atoms decrease relatively much less rapidly with increasing θ than do those for light atoms. Thus when one oxygen atom overlaps the tungsten atom in the $0kl$ projection (as was later found to be the case) n^2_{Yt} changed only from 0·98(7) to 1·07(10).

All the refinements in table IV were also carried out allotting individual isotropic temperature factors to each atom. This did not reduce the residual errors significantly and, apart from a marked increase in $\sigma(n)$, the parameters were unchanged.

Derivation of the ideal structure. Taking the tungsten atom positions in yttrotungstite as (0·184, 0·063, 0·204) in $P2_1/m$ (averaged from table IV), the tungsten atoms form a planar zig-zag up the two-fold screw axis through the origin in a plane close[1] to $(10\bar{1})$ as shown in fig. 5a. Their calculated separations are both close to 3·2 Å. Reference to many summaries given in Structure Reports (Oosthoeck, Utrecht) shows that most of the structures reported for tungsten–oxygen compounds are based only on observed tungsten positions, oxygen positions being inferred from steric considerations. In particular, a W–W separation of 3·2 Å is typical of two WO_6 octahedra sharing an edge. With the help of a packing model the oxygens thus implied here are easily located, as shown in fig. 5b; a polyhedral diagram is given in fig. 5c. Such chains have formula $(WO_4)_n$ and evidently consist of close-packed oxygens, three rows wide and two layers thick. There are gaps in the outer rows of oxygens (fig. 5b, lower half) sufficient to accommodate extra oxygens, O(6), on the mirror planes, unbonded to tungsten, raising the located unit cell contents to $(W, etc.)_4O_{18}$; it remains to locate $(Yt, etc.)_2$ and the hydrogens.

The W_4O_{18} chains are lined up in parallel so that the oxygens are in face-centred cubic array, to form 'walls' as shown in fig. 6a viewed down [010]. The walls have corrugated surfaces with protruding close-packed rows consisting of O(3) and O(6)

[1] The plane would be exactly $(10\bar{1})$ if $z_W = x_W$.

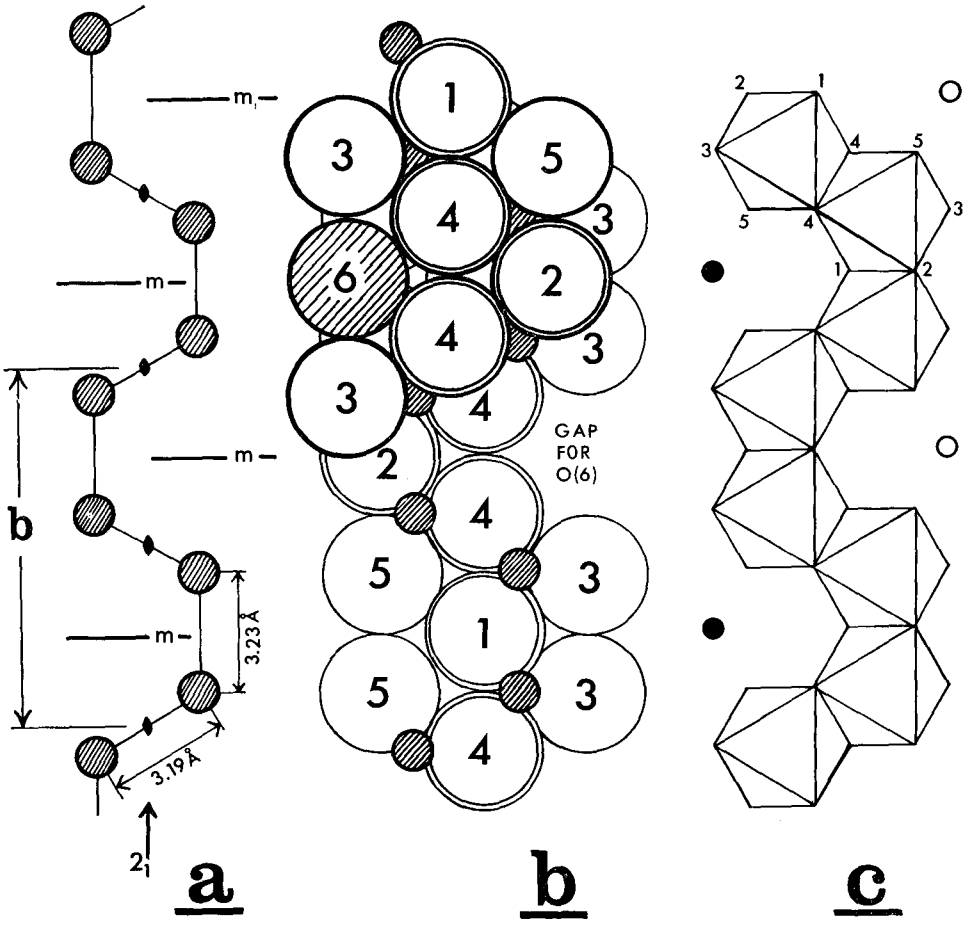

FIG. 5. Projection of the yttrotungstite structure on the plane of the tungsten atoms. (a) shows the chain of tungsten atoms (small shaded circles) zig-zagging up the *b* axis, which is a two-fold screw axis, with symmetry centres at $y = 0, \frac{1}{2}, 1$, etc. and mirror planes, *m*, at $y = \frac{1}{4}, \frac{3}{4}$, etc. (b) is a packing drawing showing how O(1) to O(5) fit round the tungsten atoms in octahedral coordination. The upper layer of oxygen atoms (heavy outline), has been omitted from the lower half of the diagram. Oxygen atoms linked to two tungsten atoms are shown in doubled outline. The extra oxygen atom O(6) is shown shaded in the upper layer and is omitted in the lower layer. (c) shows the same arrangement as a polyhedral diagram of octahedra sharing edges. Positions for O(6) are indicated by circles: filled circles for the upper layer of oxygen atoms and open circles for the lower layer.

(cf. fig. 5b), between which corresponding rows of the next wall will fit. The left-hand half of fig. 6b shows two walls fitting in this way, while the right-hand wall is in the twinned position showing the ease with which a reflection twin on {100} is formed. The yttrium atoms are now shown close to the position given by table IV, nestling on the mirror plane in the dimple between O(3), O(4″), and O(5′). Together with the corresponding atoms above the mirror plane, O(3), O(4″), and O(5′) are in trigonal

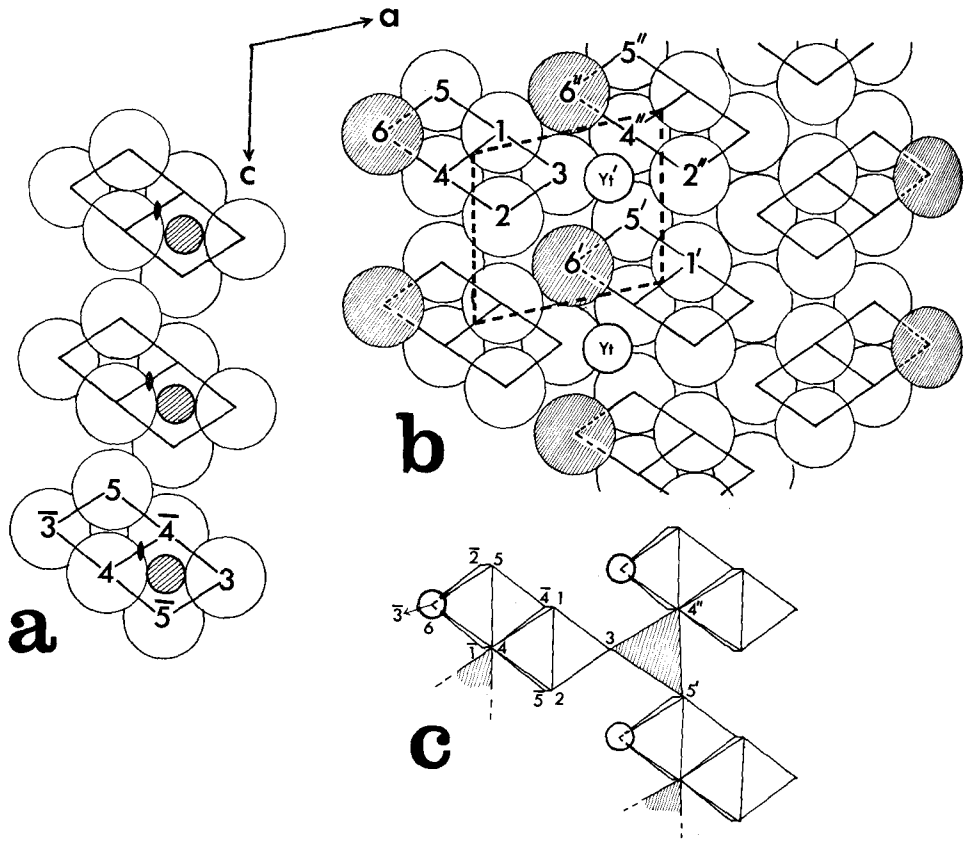

FIG. 6. Cross-sections through the yttrotungstite structure on (010). (a) shows how three chains as in fig. 5b stack together in cubic close packing to form a 'wall'. Separate chains are indicated by parallelograms (double rhombi) and, for clarity, are spaced not quite in contact. The cross-section is taken at $y = 1/12$ to show tungsten atoms (small shaded circles). Bars over oxygen-atom numbers indicate atoms related to those with unbarred numbers by the centre of symmetry at the mid-point of O(4) and O($\bar{4}$). (b) shows how three walls fit together. The cross-section is here taken at $y = \frac{1}{4}$ to show the yttrium atoms, Yt′, Yt, etc. O($\bar{4}$), O($\bar{5}$), and W in (a) are now obscured by O(1) and O(2); O($\bar{3}$) in (a) is now obscured by O(6). Axial directions are shown at the top and a unit cell is outlined in heavy dashed lines. Different chains are distinguished by unprimed, primed, and double-primed oxygen-atom numbers. The left-hand and centre walls fit together normally as in the crystal. The right-hand wall is shown related to the centre wall by a twinning plane on (100). (c) shows a section through the polyhedral diagram, taken at $y = \frac{1}{4}$ as in (b). The bases of the trigonal prisms round Yt′, Yt, etc. are shaded. The prisms link the spine of one chain with the extremities of two others. Circles show O(6), water molecules.

prismatic coordination around the yttrium atom Yt′ (cf. fig. 7a). Apart from the hydrogen atoms, the ideal structure is thus completely determined in the manner commonly reported for tungsten–oxygen compounds.

Qualitatively, this structure gives a satisfying explanation of many observations about yttrotungstite. Thus from fig. 6 the crystals are flattened parallel to the walls on {100}, although it is perhaps surprising that they are elongated perpendicular

to the chain axis along [010]. From fig. 6 the ease of twinning on {100} can be readily explained, and it can be seen that on the plane of twinning the yttrium positions are disturbed, thus making it plausible that the twinning should be on a gross, rather than a fine, scale. Easy cleavage on (010) can be explained as parting at $y = 0$ (cf. fig. 5) when only W–O bonds are broken in a manner that might be formulated as

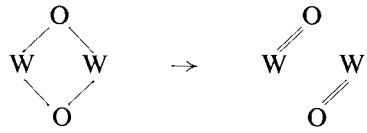

The plane {10$\bar{1}$} is plausible for the other cleavage, since it involves parting between chains in a wall, with bond-breaking of the kind:

In both these cases it is assumed that the coordination number of a tungsten atom at the newly cleaved surface can be reduced with a rearrangement of electrons involving little energy change.

From fig. 6b, $a \sin \beta$ is equivalent to three close-packed planes of oxygens and, since the unit cell in this projection is three oxygen atoms high, {110} is a close-packed plane within the face-centred cubic array of oxygen atoms in a wall, and is thus a plausible plane to bevel the laths. {10$\bar{1}$} is the plane of the surface of a chain, and is thus a plausible terminal face. It was shown above that $\gamma = [010]$ and $\alpha:[001] = 26°$, bringing the high refractive indices, β and γ, into a plane inclined at 64° to [001]. If $\alpha:[001]$ is in β acute, this plane is very close to the plane of a chain, whose strained W–O bonds to shared edges of WO_6 octahedra may well contribute to the higher refractive indices.

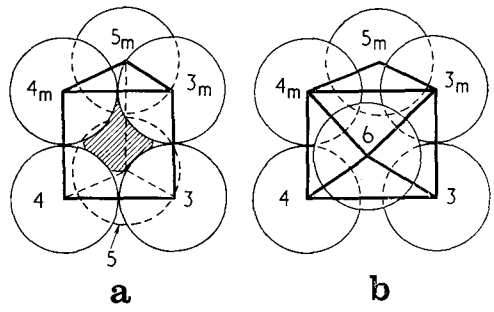

FIG. 7. (a) shows yttrium (shaded) in trigonal prismatic coordination with O(3), O(4), and O(5) (the last nearly obscured), together with the mirror-plane related oxygen atoms $O(3_m)$, $O(4_m)$, and $O(5_m)$. (b) shows the effect of adding a seventh co-ordinating oxygen atom O(6) to the front face of the prism. O(5) and yttrium are here omitted for clarity.

Coordination. Tungsten is octahedrally coordinated by O(1), O(2), O(3), 2 O(4), and O(5). Non-opposite edges, O(1) and O(2) on the mirror plane and O(4), O($\bar{4}$) bisected by the centre of symmetry, are shared with neighbouring octahedra. The octahedra cannot, however, be exactly regular. The unit cell is three oxygens high along [010], giving an average O–O separation in this direction of $b/3 = 2{\cdot}86$ Å along the chains.

For a normal W–O bond of about 1·80 Å, the O–O separation in a regular WO_6 octahedron is only $2{\cdot}54_6$ Å. The chains are evidently elongated by W–W repulsion across shared octahedral edges, so that these edges are shorter, and the chains longer, than indicated by uniform O–O separations.

The microprobe results and the cation radii show that the silicon replaces tungsten.[1] This might be taken as implying SiO_6 octahedra, for which there is some precedent in stishovite (SiO_2, rutile structure, Stishov and Belov, 1962; cf. Lyon, 1962, for infra-red data). However, this is not necessarily so. The tetrahedral Si–O bond (1·62 Å, Smith and Bailey, 1963) is little more than half the W–W separation suggesting that around Si replacing W one oxygen might be omitted from each shared edge of the octahedron, lowering the coordination number of Si to 4, and of adjacent tungsten atoms to 5, with little strain in the structure. This involves a local deficit of two oxygens per silicon atom, and we are interested to note that the analytical data of table III shows 0·07 Si atoms per cell and a deficit of 0·14 O atoms below 18 per cell. A better estimate of the oxygen deficit is obtained by incorporating H_2O- into the analysis and normalizing to exactly 6 cations per cell, when the oxygen deficit is 0·15 atoms per cell, equivalent to 0·22 wt. % H_2O.

In the ideal structure O(1) and O(2) are bonded to two tungsten atoms, O(3) and O(5) to an yttrium and a tungsten atom, and O(4) both to an yttrium and to two tungsten atoms. O(6) is not bonded to a cation and is best explained as a water molecule, causing the 6·1 μm band in the infra-red spectrum; O(6) is well embedded in the structure, explaining the high temperature required to remove it (cf. fig. 4). This accounts for four of the hydrogen atoms per unit cell. From fig. 4 and table IV, 0·51 hydrogen atoms per unit cell are lost below 200 °C and 6·11 hydrogen atoms per unit cell are lost between 250° and 600 °C. This suggests that there are two additional hydrogen atoms per unit cell forming strongly bound hydroxyl groups, probably on O(1) or O(2), besides the water molecule at O(6), giving an ideal formula for yttrotungstite of $Yt_2W_4O_{14}(OH)_2.2H_2O$.

Yttrium, Yt′, is in trigonal prismatic coordination with 2 O(3), 2 O(4″), and 2 O(5′) with the oxygens well spaced apart. For trigonal prismatic coordination, the ratio Yt–O:O–O is $\sqrt{(7/12)} = 0{\cdot}7638$; a representative value[2] of the Yt–O bond length is 2·4 Å, giving O–O = 3·14 Å, a value differing little from the van der Waals separation between unbonded oxygens. It follows from this and from the tungsten coordination that fig. 6 differs from reality; in the real structure the oxygens are nearer to the tungstens, and further from those in neighbouring chains than indicated in fig. 6b. From fig. 6c it can be seen that the yttrium–oxygen polyhedra act as 'spacers' between chains, and are thus unrestricted in size by the rest of the structure. This explains Butler's observation that the rare earths in yttrotungstite have not been fractionated according to atomic radius.

Fig. 7a shows oxygens in trigonal prismatic coordination. For convenience they

[1] We have considered the possibility of unoccupied interstitial sites for the silicon, but this would always involve large changes in cell dimensions, not observed in table I.

[2] Based on a survey of recently determined structures of yttrium–oxygen compounds (yttrium mainly 8- or 9-coordinated); subject to an error of 0·1 Å.

are drawn in contact, but even so there is a relatively large 'window' in the middle of each square prism face through which the central yttrium atom can be seen. This suggests that the coordination number of the yttrium could easily be raised above six by adding an extra oxygen at the centre of one or more of the square prism faces. We have considered an ideal case where one extra oxygen is added (fig. 7b), forcing apart O(3), O(4) and O(3_m), O(4_m) until all Yt–O separations are equal, and retaining all other oxygens in contact. For this case we calculate Yt–O:O–O as 0·780776, whence Yt–O = 2·4 Å, O–O = 3·0_7 Å. These values differ little from those derived for the trigonal prism and evidently the seventh oxygen neighbour can be accommodated without strain. For use below we also calculate the angle between the square and the triangular prism faces in fig. 7b as 68°10′.

Derivation of the real structure. The shortcomings of fig. 6 in relation to non-uniform O–O separations have been discussed above. Nevertheless, we have found it instructive to make detailed calculations on it, although these assume a uniform O–O separation, taken here as u = 2·86 Å (= $b/3$). The essential features of fig. 6b are extracted for convenient reference in fig. 8; A, B, C, D, E, F, are the projections of the centres of O(2), O(4), O(6), O(3), O(1), and O(5) respectively, and each represents a column of close-packed oxygens perpendicular to the plane of the paper; neighbouring similar chains are indicated by primes, as in fig. 6b. Neighbouring pairs of columns of oxygens in contact are of two kinds: either they contain oxygens at similar heights, e.g. O(1), O(2) in fig. 6b, when their projections are separated by u (AE in fig. 8); or their oxygens are at staggered heights, e.g. O(1), O(3) and O(2), O(3) in fig. 6b, when they overlap and are separated by $v = \frac{1}{2}\sqrt{3}\,u$ (DE, AD in fig. 8).

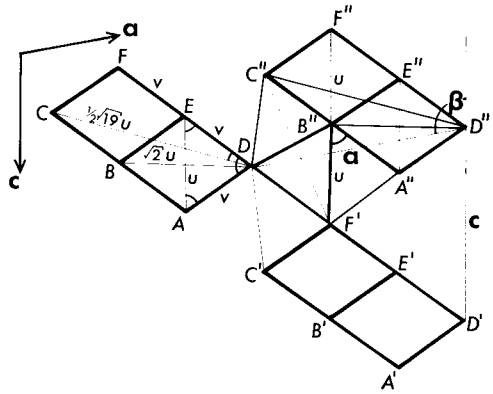

FIG. 8. Diagram to illustrate the calculations for fig. 9 (see text). The parallelograms (double rhombi) in heavy outline are taken from the numbered chains in fig. 6b. For case (i) △DF′B″ is equilateral of side u; for case (ii) C″D = v, B″D = F′B″ = u < F′D; for case (iii) C′D = v, F′D = u < B″D; for case (iv) DF′ = F′B″ = u < DB″, C″D = v.

In fig. 6b, chain parallelograms are exactly parallel to [101] whence $z_W = x_W$. Reference to a packing model shows that O(3) fits loosely between O(6′) and O(6″), being staggered in its column relative to them. The walls in fig. 6a can thus shear relative to each other, leading to non-collinear chain parallelograms and $z_W \neq x_W$. We distinguish three cases: (i) yttrium has perfect trigonal prismatic coordination, and $z_W:x_W$ = 1·10; or (ii) O(3) and O(6″) are in staggered contact, and $z_W:x_W$ = 1·00; or (iii) O(3) and O(6′) are in staggered contact, and $z_W:x_W$ = 1·31. The second and third possibilities represent extreme limits of shear between walls and the first is an intermediate case.

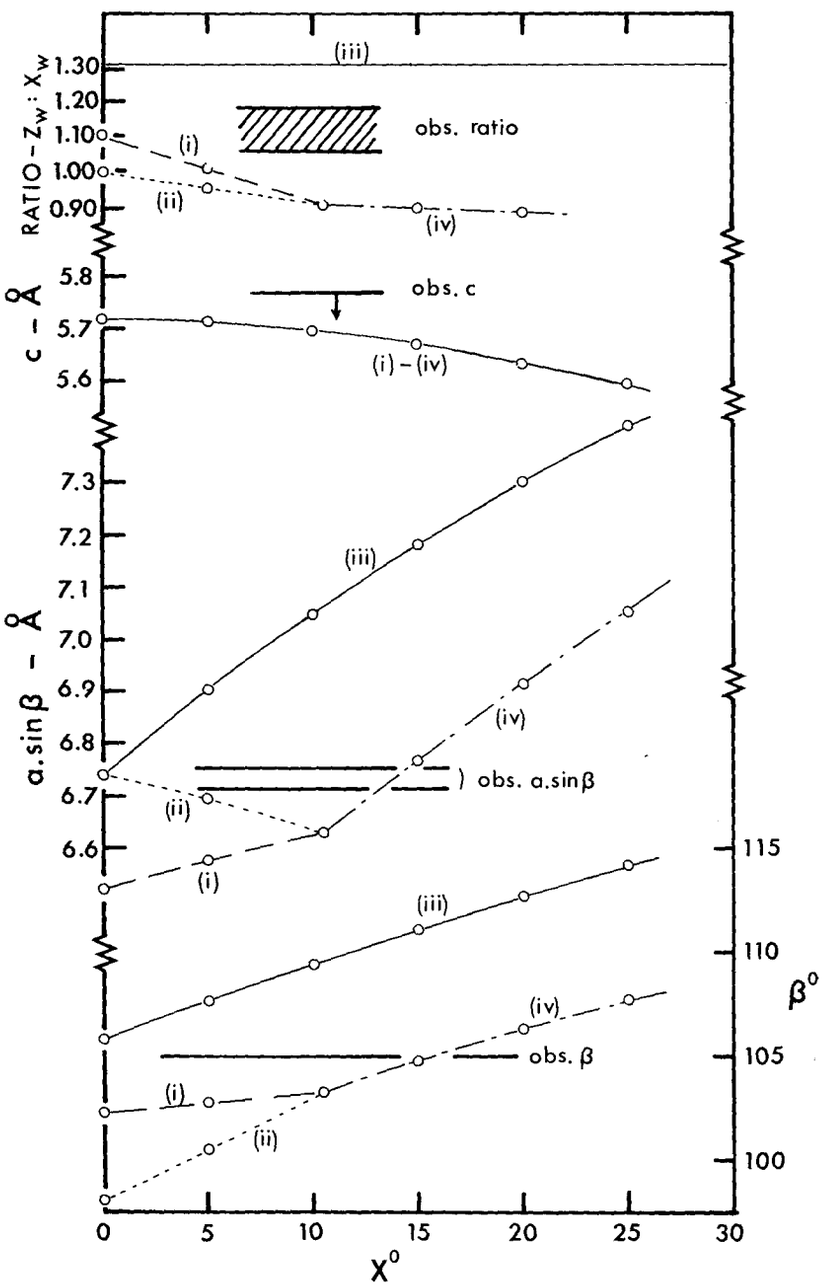

FIG. 9. Calculated values of $z_w : x_w$, c (Å), $a \sin \beta$ (Å), and β° for various values of the shear angle X.